Letter

Sub-recoil transverse momentum width in a cold ytterbium atomic beam

Toshiyuki Hosoya [1,2] Tomoya Sato [3] Ryotaro Inoue [3,*] and Mikio Kozuma [2,3,†]
[1] *Product Development Center, Japan Aviation Electronics Industry, Ltd., 3-1-1, Musashino, Akishima-shi, Tokyo 196-8555, Japan*
[2] *Department of Physics, Institute of Science Tokyo, 2-12-1 Ookayama, Meguro-ku, Tokyo 152-8550, Japan*
[3] *Institute of Integrated Research, Institute of Science Tokyo, 4259 Nagatsuta-cho, Midori-ku, Yokohama, Kanagawa 226-8501, Japan*

(Received 13 May 2025; accepted 22 September 2025; published 10 October 2025)

We demonstrate the generation of a slow ytterbium atomic beam with a transverse momentum width of 0.44(6) times the photon recoil associated with Bragg diffraction, and a flux of $6.7(9) \times 10^6$ atoms/s. This is achieved by applying momentum filtering through a long-lived metastable state to atoms prepared in a slow beam via two-dimensional transverse laser cooling. The resulting narrow momentum distribution enables efficient quasi-Bragg diffraction, which we exploit to realize a Bragg interferometer. These results mark a significant step toward continuous, high-precision, and magnetically insensitive angular rate measurements using cold alkaline-earth(-like) atomic beams.

DOI: 10.1103/4rkj-z4qp

Since the Sagnac phase shift induced by rotation is proportional to the energy of the particles involved [1], extensive research has focused on developing highly sensitive gyroscopes based on atomic interferometers as alternatives to conventional light-based systems. Atom-interferometry-based gyroscopes [2–4] have a wide range of potential applications, including precise inertial navigation [5] and tests of relativistic theories such as the geodetic and Lense-Thirring effects [6–8]. Particularly for inertial navigation, dead-time-free measurement, recently demonstrated using an atomic fountain interferometer [9], is indispensable, as the vehicle's orientation must be continuously tracked. Cold atomic beam interferometers have been intensively investigated, as they enable not only continuous measurements but also high measurement bandwidth. Such capabilities are essential for realizing practical inertial navigation systems. Recently, techniques for generating cold atomic beams using alkali atoms have been established [10,11], enabling the development of atomic interferometers based on these beams [12,13]. One of the next major challenges is to improve robustness against environmental magnetic fields to ensure high stability in field applications. A promising approach is to generate cold atomic beams of alkaline-earth(-like) atoms such as strontium or ytterbium (Yb) [14,15], and to construct atomic interferometers using Bragg diffraction, taking advantage of the magnetic insensitivity of the $^1S_0$ ground state.

The interaction time required for Bragg diffraction can be significantly reduced by employing quasi-Bragg diffraction with a Gaussian pulse [16]. This approach increases the momentum width over which diffraction can occur; however, achieving efficient Bragg diffraction still requires a momentum width narrower than the photon recoil [17]. Methods such as evaporative cooling [18] or momentum selection using quasi-Bragg diffraction itself, applied after Doppler cooling with ultranarrow transitions [19,20], have been employed to meet this requirement. Nonetheless, generating a continuous cold atomic beam using these methods remains challenging due to the long cooling times involved. Mechanical slits can, in principle, yield a cold atomic beam with a narrow transverse momentum width [21], but this method significantly restricts the atomic flux. Although state-of-the-art laser cooling with optical dipole traps can produce atoms with sub-recoil transverse momentum widths, the achievable flux remains limited to the order of 10^4 atoms/s [22]. Alternatively, coherent population trapping techniques [23] can cool atoms without significant flux loss; however, they require sublevels in the ground state, which are absent in atoms with a zero magnetic moment, such as those considered here.

In this Letter, we report the first realization of a slow Yb atomic beam with a sub-recoil transverse momentum width, achieved by momentum filtering through a long-lived metastable state applied to a cold beam prepared by two-dimensional transverse laser cooling [24]. We also demonstrate higher-order quasi-Bragg diffraction and a Bragg interferometer utilizing this continuous atomic beam.

Figure 1 describes the concept of a momentum filtering scheme. Although Yb is used for illustration, the method can be readily applied to other atomic species with suitable metastable states. An excitation laser beam resonant with the ultranarrow $^1S_0$–$^3P_2$ transition (wavelength: 507 nm, natural linewidth: 25 mHz [25]) is introduced orthogonally to the atomic beam, which has a transverse momentum width broader than the photon recoil $\hbar k_{399}$ of the Bragg light tuned to the dipole-allowed $^1S_0$–$^1P_1$ transition (wavelength: 399 nm,

*Present address: Nanofiber Quantum Technologies, Inc.
†Contact author: kozuma@qnav.iir.isct.ac.jp

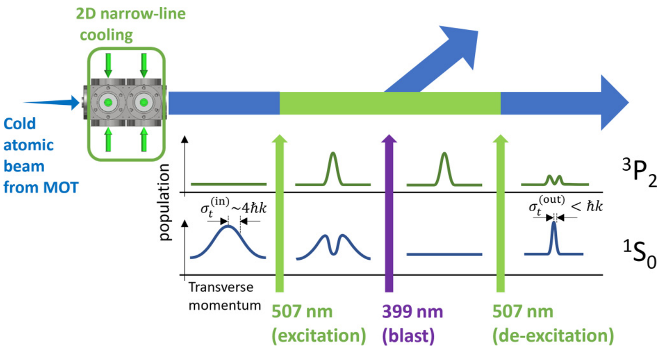

FIG. 1. The concept of a momentum filtering scheme. A pre-cooled atomic beam is irradiated with 507 nm light to excite atoms with transverse momentum below the photon recoil into the $^3P_2$ state. Atoms remaining in $^1S_0$ are removed with 399 nm light, and the filtered atoms are returned to $^1S_0$ by a second 507 nm pulse. The thick arrow in the figure represents the propagation of the atomic beam in real space.

natural linewidth: 29 MHz [26]). Here, k_{399} is the wavenumber of the Bragg light. Although the $^3P_0$ state could be used instead of the $^3P_2$ state, in the present experiment, we selected the $^3P_2$ state in view of the required laser power and the relative ease of preparing high-power laser sources at the transition wavelength.

A portion of the incoming atoms in the ground $^1S_0$ state is selectively excited to the metastable $^3P_2$ state via interaction with a continuous Gaussian excitation beam. The remaining atoms in the ground state are removed by a subsequently applied blast beam at 399 nm. A deexcitation laser beam then selectively transfers the atoms in the metastable state back to the ground state in momentum space. The excitation and deexcitation laser beams exhibit Gaussian interaction profiles with identical beam waists w_e. The transit time of w_e/v leads to a broadening of the excitation spectrum, where v denotes the atomic longitudinal velocity. The corresponding Gaussian root-mean-square (rms) momentum width is given by $\sigma_t = Mv/(k_{507}w_e)$, where M is the atomic mass and k_{507} is the wavenumber of the 507 nm excitation and deexcitation lasers [27]. To achieve efficient excitation and deexcitation of the $^1S_0$–$^3P_2$ transition, the power broadening at the center of the excitation/deexcitation beam is set to $\sqrt{2\pi}$ times the transit-time broadening. The momentum width of atoms transferred by the Gaussian pulse is predominantly determined by σ_t, as verified through optical Bloch equation simulations. The transverse momentum width of the final atomic beam can be expressed as $\sigma_t^{(out)} = \sigma_t/\sqrt{2 + (\sigma_t/\sigma_t^{(in)})^2}$, where $\sigma_t^{(in)}$ denotes the rms transverse momentum width of the incident atomic beam.

A technique for measuring the transverse momentum distribution of an atomic beam is essential not only for verifying momentum filtering, but also for the implementation of Bragg diffraction and atom interferometry. Figure 2(a) illustrates the momentum-resolving detection scheme. A similar probing technique was employed by Curtis *et al.* in cold Ca atomic gases [28]. A momentum selection beam, detuned by δ_m from the resonance frequency ω_0 of the ultranarrow 507 nm transition, is applied orthogonally to the atomic beam. The atomic beam with its transverse momentum of $M\delta_m/k_{507}$ is

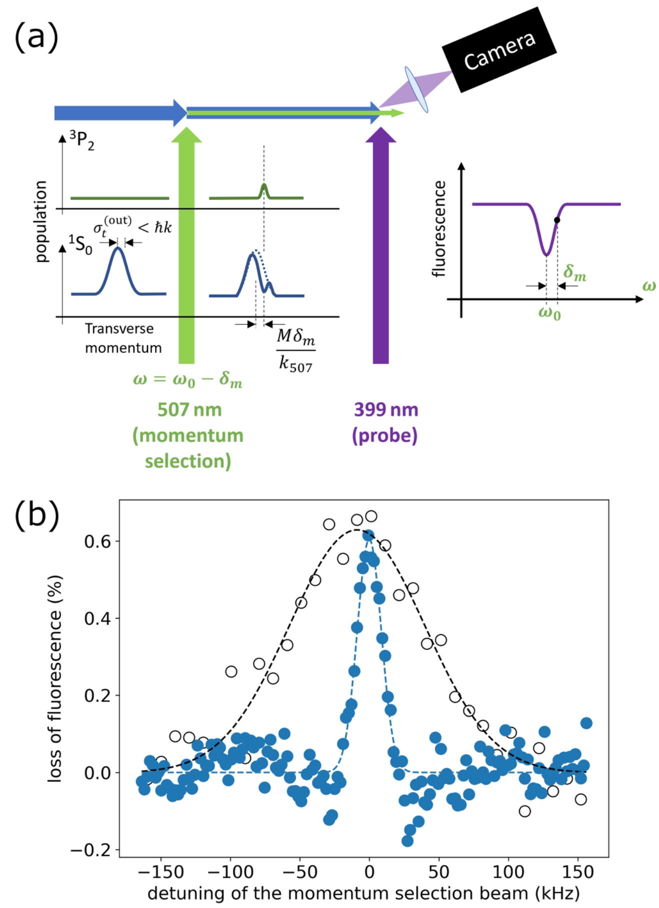

FIG. 2. (a) Schematic view of the momentum-resolving detection. (b) Dependence of fluorescence loss on the detuning of the momentum-selection beam, shown without (black open circles) and with (blue filled circles) momentum filtering. Dashed lines indicate least-squares fits to the data.

selectively excited to the metastable state. When a probe beam resonant with the dipole-allowed transition (399 nm) is subsequently applied to the atomic beam, fluorescence from the atoms decreases as a portion of the atoms transitions from the ground state to the metastable state. The overall momentum distribution can be extracted from the fluorescence reduction by scanning the frequency of the momentum selection beam.

For the demonstration of the method, we prepared ^{171}Yb atomic beam, which requires less optical power for the transition from $^1S_0$ to $^3P_2$ [24], though essentially our method can be applied to the bosonic isotopes, such as ^{174}Yb. A continuous atomic beam of ^{171}Yb, characterized by a typical transverse momentum width of $4\hbar k_{399}$ and a longitudinal velocity v of approximately 30 m/s, was generated through laser cooling using a combination of the dipole-allowed transition at 399 nm and the $^1S_0$–$^3P_1$ intercombination transition at 556 nm, as described in Ref. [24]. Note that the atomic beam comprised atoms in two nuclear spin sublevels ($I = 1/2, m_I = \pm 1/2$). In our setup, a magnetic field of 10^{-5} T is applied during the momentum filtering process, inducing Zeeman splitting of the magnetic sublevels. As a result, the filtering process selectively targets atoms in the $m_I = +1/2$ state, utilizing σ_+-polarized light for both excitation and deexcitation. The beam waist of both the excitation and deexcitation beams was set to $w_e = 1.1$ mm, which is expected to yield a filtered transverse momentum width of $\sigma_t^{(\text{out})} = 0.27\,\hbar k_{399}$. Note that the linewidth of the 507 nm laser is about 200 Hz, which is much narrower than the 3 kHz Doppler width corresponding to the target momentum width. While it is preferable for the vertical beam waists of the excitation and deexcitation beams to exceed the $1/e^2$ radius (i.e., 2σ) of the atomic beam, which is 1.9 mm at the position of the laser beams, they were constrained to 1.1 mm—the same as in the horizontal direction—due to the limited available laser power of 500 mW. This issue can be fundamentally addressed by interacting the atoms with 507 nm light whose effective power is enhanced by a bow-tie (or similar) enhancement cavity.

To verify the effectiveness of our momentum filtering, we used a probe beam with a waist $w_p = 0.3$ mm, much smaller than the atomic beam's $1/e^2$ radius of 3.1 mm at the probe position. In Fig. 2(b), the maximum fluorescence loss in the momentum-filtered case reaches that of the unfiltered one, indicating a nearly 100% filtering efficiency. This high efficiency arises because the probe light interacted with atoms passing near the center of the excitation and deexcitation beams, where the π-pulse condition was satisfied. In this sense, this is local filtering effectiveness under idealized overlap. Figure 2(b) clearly shows that the filtering process effectively reduced the transverse momentum width of the atomic beam. The Gaussian standard deviations of the measured spectra without and with filtering were 48.7(3.0) and 8.7(0.4) kHz, respectively. After accounting for the transit-time broadening of 7.1 kHz associated with momentum-selective detection, the standard deviations of the spectra attributable to the atomic momentum width are estimated to be 48.2(3.0) and 5.0(0.7) kHz, respectively. These correspond to transverse momentum widths of $4.3(0.3)\hbar k_{399}$ and $0.44(6)\hbar k_{399}$, respectively. The measured value exceeds the theoretical prediction of $0.27\hbar k_{399}$, calculated from the atomic beam velocity v and the longitudinal beam waist w_e of the excitation and deexcitation beams. One possible cause of the discrepancy between the experimental results and the theoretical predictions is the presence of a residual ac magnetic field at the positions of the excitation and deexcitation beams. A field as small as 10^{-7} T is sufficient to broaden the momentum width to $0.44\,\hbar k_{399}$. An ac magnetic field arising from temporal variations, for example, those associated with commercial power lines or laboratory equipment, can account for such fluctuations.

To estimate the atomic flux after momentum filtering, we measured the fluorescence ratio with and without the filtering process, omitting the momentum selection step. A probe beam with a top-hat intensity profile was used, with vertical and horizontal dimensions of 7.5 and 2.5 mm, respectively. The vertical size exceeded the $1/e^2$ radius (3.1 mm) of the atomic beam, ensuring complete spatial overlap. The fluorescence ratio with and without filtering was measured to be 2.9(2)%. The total atomic flux was independently determined using conventional absorption spectroscopy to be $2.3(3) \times 10^8$ atoms/s. Based on the measured fluorescence ratio, the atomic flux after momentum filtering was estimated to be $6.7(9) \times 10^6$ atoms/s. Assuming ideal filtering within a transverse momentum window of $0.44\,\hbar k_{399}$ from an initial momentum distribution width of $4.3\,\hbar k_{399}$, the expected atomic flux would be $1.2(2) \times 10^7$ atoms/s. The experimentally observed filtering efficiency of 56(5)% is expected to approach unity with increased optical power and larger vertical beam waists for both excitation and deexcitation beams. This value corresponds not to the local filtering effectiveness under idealized overlap discussed earlier, but to the filtering efficiency in our experimental setup.

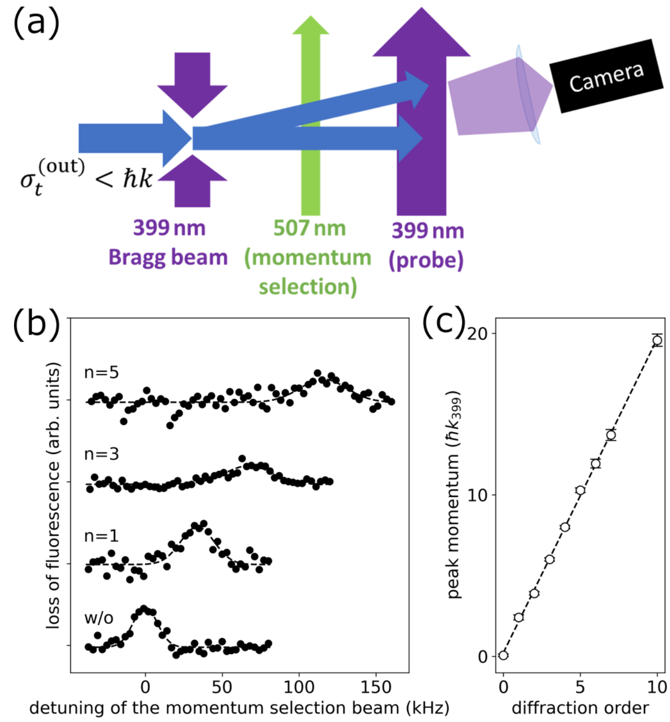

FIG. 3. (a) Schematic view of the setup for the Bragg diffraction experiment. (b) Obtained loss in the momentum-resolving detection for each setting for the diffraction order. Dashed lines are fitting curves obtained by the least-square method. (c) The dependence of the momentum transfer on the Bragg order.

We observed quasi-Bragg diffraction using a cold Yb atomic beam with a transverse momentum width below the recoil limit. Figure 3(a) shows the experimental setup for the Bragg diffraction. Bragg beams, consisting of a pair of counter-propagating laser beams with a frequency difference of δ_n, are applied orthogonally to the incoming cold atomic beam, where $\delta_n = 4n\omega_r$, with n denoting the diffraction order and ω_r the recoil frequency. Quasi-Bragg diffraction imparts a momentum transfer of $2n\hbar k_{399}$ to the atom, while leaving the atom in its internal ground state. The postdiffraction momentum distribution was measured via the momentum-selective detection scheme illustrated by Fig. 2(a). The horizontal and vertical waists of the Bragg beam were 0.25 and 2.5 mm, respectively. The detuning was set to −20 GHz relative to the ${}^1S_0$–${}^1P_1$ transition. The laser power was optimized to maximize the efficiency of each Bragg diffraction order; for example, a power of 25 mW was used for third-order quasi-Bragg diffraction. The narrow transverse momentum width of the atomic beam allows individual diffraction orders to be resolved [Figs. 3(b) and 3(c)]. Note that without momentum filtering, the population difference between the $0\hbar k_{399}$ and $2\hbar k_{399}$ states is only about 10%, making it difficult to observe a clear Bragg diffraction signal.

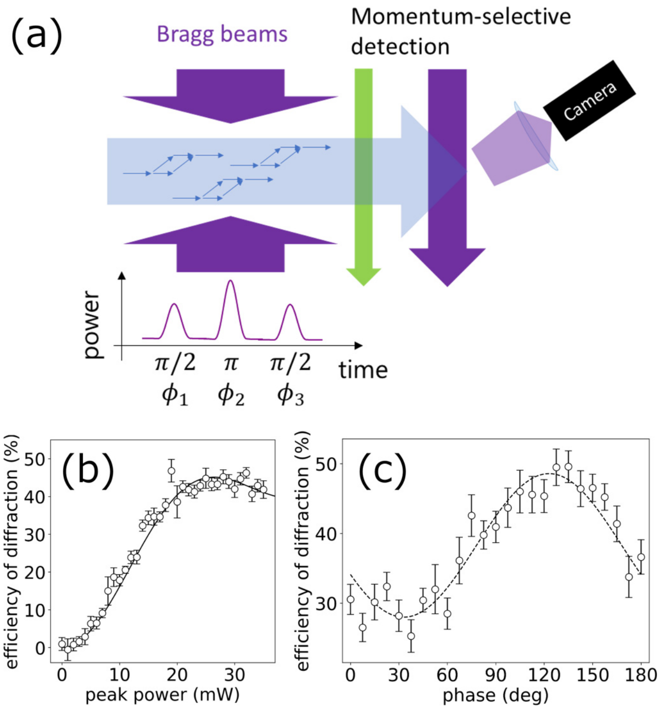

FIG. 4. (a) Schematic view of the setup for the Bragg interferometer experiment. (b) The dependence of the diffraction efficiency on the power of Bragg light. The solid line is the theoretical calculation for current experimental parameters. (c) The dependence of the population in $2\hbar k_{399}$ momentum state on the phase of the central π pulse. Dashed line is the least-square fitting with a sinusoidal function.

Finally, we demonstrated a Mach-Zehnder interferometer (MZI) based on quasi-Bragg diffraction using a momentum-filtered atomic beam [see Fig. 4(a)]. While spatial-domain MZIs with continuous atomic beams require three phase-synchronized Bragg beams, a time-domain MZI [18] can be realized with a single beam. We adopted this simpler approach for our demonstration with a slow atomic beam. The Bragg light field was formed by counter-propagating top-hat beams with a frequency offset. A precisely timed sequence of $\pi/2$–π–$\pi/2$ pulses acted as the beam splitter and mirror, completing the interferometer. Since uniform wavefronts and intensity over the entire sequence are essential to ensure coherent manipulation of the atomic ensemble, we used a beam shaper to generate a 7.5-mm diameter top-hat beam, similar to the method in Ref. [29]. The $\pi/2$–π–$\pi/2$ pulse sequence had to be completed within a duration much shorter than the time required for the atoms to traverse the entire Bragg beam area (250 µs). To satisfy this condition, a pulse with a standard deviation of 3.5 µs was employed, although the optimal pulse width for quasi-Bragg diffraction is estimated to be 7 µs. The time interval between pulses was set to 24.5 µs, resulting in a total sequence duration of 73.5 µs. To increase the number of atoms participating in the MZI, the $\pi/2$-π-$\pi/2$ pulse sequence was repeated every 250 µs. The temporal profile of the optical pulses was controlled using acousto-optic modulators (AOMs) placed in both counter-propagating Bragg beams.

We first observed Rabi oscillations between $0\hbar k_{399}$ and $2\hbar k_{399}$ using a single Bragg pulse [Fig. 4(b)], along with momentum-resolved detection as described previously. The observed power dependence of the population was consistent with theoretical calculations, allowing us to estimate the appropriate laser powers for the $\pi/2$ and π pulses. In the experiment, we employed powers of 15 and 20 mW with a detuning of -4.5 GHz, while numerical calculations predicted optimal powers of 15 and 22 mW, respectively. The output phase of the MZI, ϕ, consists of the inertial phase shift ϕ_{inertial}, arising from acceleration and rotation, and the phases of the three Bragg pulses, ϕ_1, ϕ_2, and ϕ_3. These are related by $\phi = \phi_{\text{inertial}} + \phi_1 - 2\phi_2 + \phi_3$. When the apparatus is stationary in the laboratory frame, ϕ_{inertial} remains constant. By varying the phase of the central π pulse, ϕ_2, from 0° to 180°—achieved by adjusting the relative phase between the two RF signals driving the AOMs—we observed a corresponding modulation in the momentum populations [see Fig. 4(c)]. The interference fringe, observed via oscillations between $0\hbar k_{399}$ and $2\hbar k_{399}$, varied at twice the phase of the second pulse, in agreement with theoretical predictions. The measured 20(2)% contrast agrees with the theoretical estimate of 23(3)%, based on the combined effects of the repetition duty cycle (0.71) and the limited single-pulse diffraction efficiency due to the 3.5 µs Bragg pulse being half of the optimal 7 µs (0.33). This reduced contrast arises from the suboptimal pulse width, which keeps the single-pulse diffraction efficiency below 50% [see Fig. 4(b)]. Using the optimal pulse duration is expected to yield contrasts exceeding 90%.

In conclusion, we implemented momentum filtering using an ultranarrow optical transition to generate an atomic beam with a sub-recoil transverse momentum width, suitable for Bragg interferometry. Applied to a laser-cooled, slow, and continuous Yb atomic beam (30 m/s, flux of $2.3(3) \times 10^8$ atoms/s), the filtering yielded a width of $0.44(6)\hbar k_{399}$ and a flux of $6.7(9) \times 10^6$ atoms/s. Using a momentum-resolved detection scheme, we achieved higher-order quasi-Bragg diffraction and demonstrated a time-domain Mach-Zehnder interferometer employing a momentum-filtered atomic beam. Based on the realized atomic beam flux and the experimentally obtained interference contrast, the angular random walk (ARW) of our present Mach-Zehnder atom interferometer is estimated to be 11 deg$\sqrt{\text{h}}$. Assuming a 100 mm arm length and using optimal quasi-Bragg diffraction beams (with an assumed contrast of about 90%), this value could be reduced to about 130 µdeg/$\sqrt{h}$. State-of-the-art fiber-optic gyroscopes, representing the current benchmark in inertial navigation, achieve ARW below 100 µdeg/$\sqrt{h}$ [30], suggesting that comparable performance could be reached with the proposed approach. Using nth order Bragg diffraction would further reduce this value by a factor of $1/n$. These results support the use of continuous, sub-recoil atom sources for precision interferometry and pave the way for inertial sensors based on alkaline-earth(-like) atoms that are inherently insensitive to magnetic field fluctuations. A low-velocity atomic beam with a narrow transverse momentum width may also be advantageous for applications such as optical frequency standards employing Ramsey-Bordé interferometry.

Acknowledgments. We are grateful to Atsushi Kira for valuable discussions. This work was supported by JST, Japan, Grants No. JPMJMI17A3 and No. JPMJPF2015. T.H.

acknowledges partial support from the Japan Society for the Promotion of Science.

Data availability. The data that support the findings of this article are openly available [31].

[1] J. F. Clauser, Ultra-high sensitivity accelerometers and gyroscopes using neutral atom matter-wave interferometry, Physica B+C **151**, 262 (1988).

[2] F. Riehle, T. Kisters, A. Witte, J. Helmcke, and C. J. Bordé, Optical Ramsey spectroscopy in a rotating frame: Sagnac effect in a matter-wave interferometer, Phys. Rev. Lett. **67**, 177 (1991).

[3] T. L. Gustavson, P. Bouyer, and M. A. Kasevich, Precision rotation measurements with an atom interferometer gyroscope, Phys. Rev. Lett. **78**, 2046 (1997).

[4] T. L. Gustavson, A. Landragin, and M. A. Kasevich, Rotation sensing with a dual atom-interferometer Sagnac gyroscope, Class. Quantum Gravity **17**, 2385 (2000).

[5] D. Titterton and J. L. Weston, *Strapdown Inertial Navigation Technology* (Institution of Engineering and Technology, London, 2004).

[6] S. Dimopoulos, P. W. Graham, J. M. Hogan, and M. A. Kasevich, General relativistic effects in atom interferometry, Phys. Rev. D **78**, 042003 (2008).

[7] J. K. Stockton, K. Takase, and M. A. Kasevich, Absolute geodetic rotation measurement using atom interferometry, Phys. Rev. Lett. **107**, 133001 (2011).

[8] M. He *et al.*, The space cold atom interferometer for testing the equivalence principle in the China Space Station, npj Microgravity **9**, 58 (2023).

[9] D. Savoie, M. Altorio, B. Fang, L. A. Sidorenkov, R. Geiger, and A. Landragin, Interleaved atom interferometry for high-sensitivity inertial measurements, Sci. Adv. **4**, eaau7948 (2018).

[10] Y. Feng, H. Xue, X. Wang, S. Chen, and Z. Zhou, Observation of Ramsey fringes using stimulated Raman transitions in a laser-cooled continuous rubidium atomic beam, Appl. Phys. B **118**, 139 (2015).

[11] J. Kwolek, C. Fancher, M. Bashkansky, and A. Black, Three-dimensional cooling of an atom-beam source for high-contrast atom interferometry, Phys. Rev. Appl. **13**, 044057 (2020).

[12] J. M. Kwolek and A. T. Black, Continuous sub-Doppler-cooled atomic beam interferometer for inertial sensing, Phys. Rev. Appl. **17**, 024061 (2022).

[13] Z.-X. Meng, P.-Q. Yan, S.-Z. Wang, X.-J. Li, H.-B. Xue, and Y.-Y. Feng, Closed-loop dual-atom-interferometer inertial sensor with continuous cold atomic beams, Phys. Rev. Appl. **21**, 034050 (2024).

[14] I. Nosske, L. Couturier, F. Hu, C. Tan, C. Qiao, J. Blume, Y. H. Jiang, P. Chen, and M. Weidemüller, Two-dimensional magneto-optical trap as a source for cold strontium atoms, Phys. Rev. A **96**, 053415 (2017).

[15] E. Wodey, R. J. Rengelink, C. Meiners, E. M. Rasel, and D. Schlippert, A robust, high-flux source of laser-cooled ytterbium atoms, J. Phys. B **54**, 035301 (2021).

[16] H. Müller, S.-W. Chiow, and S. Chu, Atom-wave diffraction between the Raman-Nath and the Bragg regime: Effective Rabi frequency, losses, and phase shifts, Phys. Rev. A **77**, 023609 (2008).

[17] S. S. Szigeti, J. E. Debs, J. J. Hope, N. P. Robins, and J. D. Close, Why momentum width matters for atom interferometry with Bragg pulses, New J. Phys. **14**, 023009 (2012).

[18] Y. Torii, Y. Suzuki, M. Kozuma, T. Sugiura, T. Kuga, L. Deng, and E. W. Hagley, Mach-Zehnder Bragg interferometer for a Bose-Einstein condensate, Phys. Rev. A **61**, 041602 (2000).

[19] H. Müller, S.-W. Chiow, Q. Long, S. Herrmann, and S. Chu, Atom interferometry with up to 24-photon-momentum-transfer beam splitters, Phys. Rev. Lett. **100**, 180405 (2008).

[20] T. Mazzoni, X. Zhang, R. Del Aguila, L. Salvi, N. Poli, and G. M. Tino, Large-momentum-transfer Bragg interferometer with strontium atoms, Phys. Rev. A **92**, 053619 (2015).

[21] D. M. Giltner, R. W. McGowan, and S. A. Lee, Atom interferometer based on Bragg scattering from standing light waves, Phys. Rev. Lett. **75**, 2638 (1995).

[22] C.-C. Chen, R. González Escudero, J. Minář, B. Pasquiou, S. Bennetts, and F. Schreck, Continuous Bose Einstein condensation, Nature (London) **606**, 683 (2022).

[23] A. Aspect, E. Arimondo, R. Kaiser, N. Vansteenkiste, and C. Cohen-Tannoudji, Laser cooling below the one-photon recoil energy by velocity-selective coherent population trapping, Phys. Rev. Lett. **61**, 826 (1988).

[24] T. Hosoya, R. Inoue, T. Sato, and M. Kozuma, High-flux cold ytterbium atomic beam source using two-dimensional laser cooling with intercombination transition, Opt. Commun. **528**, 129048 (2023).

[25] S. G. Porsev and A. Derevianko, Hyperfine quenching of the metastable $^3P_{0,2}$ states in divalent atoms, Phys. Rev. A **69**, 042506 (2004).

[26] Y. Takasu, K. Komori, K. Honda, M. Kumakura, T. Yabuzaki, and Y. Takahashi, Photoassociation spectroscopy of laser-cooled ytterbium atoms, Phys. Rev. Lett. **93**, 123202 (2004).

[27] W. Demtröder, *Laser Spectroscopy* (Springer, Berlin, Heidelberg, 1981), Vol. 5.

[28] E. A. Curtis, C. W. Oates, and L. Hollberg, Quenched narrow-line laser cooling of ^{40}Ca to near the photon recoil limit, Phys. Rev. A **64**, 031403(R) (2001).

[29] N. Mielec, M. Altorio, R. Sapam, D. Horville, D. Holleville, L. A. Sidorenkov, A. Landragin, and R. Geiger, Atom interferometry with top-hat laser beams, Appl. Phys. Lett. **113**, 161108 (2018).

[30] Y. Paturel, J. Honthaas, H. Lefèvre, and F. Napolitano, One nautical mile per month fog-based strapdown inertial navigation system: A dream already within reach?, Gyroscopy Navig. **5**, 1 (2014).

[31] T. Hosoya, Data for sub-recoil transverse momentum width in a cold ytterbium atomic beam [Data set], Zenodo, (2025), https://doi.org/10.5281/zenodo.15393456.